Continuum of metastable helical states of monoaxial chiral magnets: effect of the boundary conditions

V. Laliena,[1] S. A. Osorio,[2,3] S. Bustingorry,[2,3,4] and J. Campo[4,5]

[1] *Department of Applied Mathematics and Institute of Mathematics and Applications (IUMA), University of Zaragoza, C/ María de Luna 3, 50018 Zaragoza, Spain*
[2] *Instituto de Nanociencia y Nanotecnología (CNEA-CONICET), Nodo Bariloche, Av. Bustillo 9500 (R8402AGP), S. C. de Bariloche, Río Negro, Argentina*
[3] *Gerencia de Física, Centro Atómico Bariloche, Av. Bustillo 9500 (R8402AGP), S. C. de Bariloche, Río Negro, Argentina*
[4] *Aragon Nanoscience and Materials Institute (CSIC-University of Zaragoza) and Condensed Matter Physics Department, University of Zaragoza, C/ Pedro Cerbuna 12, 50009 Zaragoza, Spain*
[5] *International Institute for Sustainability with Knotted and Chiral Meta Matter (Visiting Professor), 2-313 Kagamiyama, Higashi-Hiroshima, Hiroshima, 739-0046, Japan*

(Dated: May 13, 2024)

In a recent publication we showed that a monoaxial chiral magnet has a continuum of metastable helical states differing by the helix wave number. This intringuing result was obtained for the case of an infinite magnet (or of a magnet with periodic boundary conditions). However, it has been pointed out that in a real magnet only one of these states is compatible with the boundary conditions, because the helix wave number is determined by the surface chiral twist. Thus, only one of the continuum of states is physically realizable. This is true for the case of a chiral magnet in contact with a non magnetic medium (vacuum or air, for instance), but the boundary conditions can be altered by setting the chiral magnet in contact with another magnetic medium, which may be able to absorb the surface chiral twist. We show here that this is indeed the case by studying a composite magnet system, which consists of one monoaxial chiral magnet of rectangular parallelepiped shape which has two similar slabs of a uniaxial ferromagnet attached to each of the faces that are perpendicular to the chiral axis. We show that, in the case of zero applied field, this composite system has a number of metastable helical states which is proportional to the length L_0 of the chiral magnet along the chiral axis, and that the results of our previous publication are recovered in the limit $L_0 \to \infty$.

I. INTRODUCTION

Chiral magnets, characterized by the presence of a sizable Dzyaloshinskii- $MnNb_3S_6$ interaction (DMI), are being extensively studied since they host noncollinear magnetic states which appear as metastable or equilibrium states at low temperature. Besides their intrinsic theoretical interest, these magnetic textures have inportant potential applications in spintronics and magnonics [1–4]. Examples of these noncollinear magnetic textures are the skyrmions of cubic chiral magnets [5, 6], the one dimensional chiral solitons of monoaxial chiral magnets [7, 8], and the helical or conical states which appear in both types of chiral magnets [8, 9].

Cubic chiral magnets have been studied in much more detail than monoaxial chiral magnets, the object of the present work, but nevertheless the main features of the equilibrium properties of the latter are rather well understood. In monoaxial chiral magnets the DMI acts only along one specific direction with coincides with one crystallographic axis. We call this direction the *chiral axis*. To set this work in its context, let us summarize briefly the equilibrium properties of monoaxial chiral magnets. At low temperature and zero applied field the equilibrium state is a helical structure whose wave number is determined by the competition between the Heisenberg exchange interaction and the DMI. When an external field is applied the helical structure becomes a conical structure if the field is parallel to the chiral axis, a chiral soliton lattice if the field is perpendicular to the chiral axis, or a magnetic structure which interpolates between these two limiting cases if the field is neither perpendicular nor parallel to the chiral axis [10–21]. If the applied field strength is high enough the equilibium state is a forced ferromagnetic state, which can host metastable isolated solitons [22]. The archetypical monoaxial helimagnet is $CrNb_3S_6$ [23, 24], but there are many others like $CrTa_3S_6$, $MnNb_3S_6$, CuB_2O_4, $CuCsCl_3$, $Yb(Ni_{1-x}Cu_x)_3Al_9$, or $Ba_2CuGe_2O_7$ [25–31].

Although in the last years the magnetic states that have received more attention and caused more excitement have been the topologically non trivial skyrmions, recently there has been a revival of the interest in the helical/conical states, since the conical phases occupy a larger fraction of the phase diagram and thus are created more easily. In cubic chiral magnets the equilibrium helical states are degenerated since the helix wave vector can point in different equivalent crystallographic directions selected by the cubic anisotropy. It has been shown that the wave vector direction can be controlled by electric means and thus helical states with different wave vectors can be used to storage and manipulate information [32]. The direction of the helix wave vector can also be changed by means of thermal currents [33]. Therefore, the orientation of helical stripes may serve as building blocks for devices for classical or unconventional computing, in what would be a new technology that may be named *helitronics* [34].

In monoaxial chiral magnets the degeneracy of the helical state is absent since the helix wave vector points along the chiral axis in the direction determined by the DMI. However, it was shown that in monoaxial chiral magnets there is a continuum of metastable helical states differing by the helix wave number [35, 36] (metastable helical states of this kind exists also in cubic chiral magnets [37]). In reference 35 we showed that it is possible to swicth between these helical states, which were called there p states, by applying magnetic fields and electric currents along the chiral axis. Therefore, these p states could serve as building blocks for computing devices.

The existence of this continuum of metastable states, differing from the equilibrium helical state only by the wave number, is an intringuing question. Theses states were obtained by solving the magnetic equilibrium equations for an infinite magnet, ignoring thus the boundary conditions. However, it has been pointed out that in a real magnet the surface chiral twist required by the boundary conditions in presence of DMI actually selects the equilibrium helical state, which is the only p state which satisfies the boundary conditions [38]. This is true for a chiral magnet which is surrounded by a non magnetic medium (air or vacuum, for instance). But if the chiral magnet is in contact with another magnet with appropriate characteristics, the surface chiral twist can be absorbed by the surrounding magnet, and the continuum of metastable p states may be present.

The purpose of this work is to show that the multiplicity of helical states is present also in a real chiral magnet, developing the ideas put froward in the end of the previous paragraph. Besides an intrinsic theoretical interest, the presence of many metastable helical states is interesting from the point of view of applications since, as explained in reference [35], they could be used in spintronics as, for instance, elementary carriers of information. For simplicity, we restrict the analysis to the case of zero applied field and zero current, because in this case the theoretical problem can be solved exactly.

The paper is organized as follows. In section II we analize carefully the conditions that the magnetization has to satisfy at the interface that separates two different media; in section III we describe a system which host a continuum of p states, which consists of a monoaxial chiral magnet of rectangular shape, with the two faces perpendicular to the chiral axis sticked to two similar slabs of a uniaxial ferromagnet; section IV is devoted to the determination of the helical states of this system and in section V the stability of these states is analyzed. Finally, in section VII we summarize the conclusions.

II. CONDITIONS AT THE INTERFACE BETWEEN THE TWO MEDIA

The magnetization of a composite magnetic system formed by several magnetic media set in contact is not a smooth function in general, but it is generically discontinuous at the interfaces, due to the discontinuity of the saturation magnetization. However, the mathematical structure of the Landau-Lifschitz-Gilbert (LLG) equation set constraints on the nature of the singularity of the magnetization. It turns out that the vector field that describe the direction of the magnetization has to be continuous at the interface, although its derivative along the normal vector of the interface may be discontinuous.

The conditions which has to satisfy the magnetization at interfaces have been obtained in reference 39 (see also reference 40) by studying the variational problem from which the LLG equation is derived. In this section we analyze these conditions directly from the LLG equation, rather than from the variational approach.

To set the notation, let the unit vectors $\hat{x} = \hat{x}_1$, $\hat{y} = \hat{x}_2$ and $\hat{z} = \hat{x}_3$ form a set of cartesian coordinate axes and let $x = x_1$, $y = x_2$, and $z = x_3$ be the corresponding coordinates. For notational convenience, to analyze the conditions on the magnetization at the interface between two different media it is convenient to work with a system which is slightly more general than that studied in this work (section III). Thus, in this section we consider an inhomogeneous magnet in which the magnetization direction is described by the unit vector field $\hat{n}$ and whose energy density is given by

$$W = \sum_{i=1}^{3} \Big(A \partial_i \hat{n} \cdot \partial_i \hat{n} - D_i \hat{n} \cdot (\hat{x}_i \times \partial_i \hat{n}) \Big) + W_0(\hat{n}), \quad (1)$$

where A and D_i are the intensities of the ferromagnetic and DMI exchange interactions, respectively. If $D_1 = D_2 = D_3$ we have a chiral cubic magnet and if $D_1 = D_2 = 0$ and $D_3 \neq 0$ we have a monoaxial chiral magnet with chiral axis along $\hat{z}$. The term W_0 contains all the terms which do not depend on the derivatives of $\hat{n}$. For instance, the single-ion anisotropy energies, the energy associated to the applied field, and the magnetostatic interaction are included in W_0.

Our goal is to study the conditions that the magnetization has to fullfill at the sharp interface between two different media, where the interaction intensities A and D_i, and the other parameters of the system, such us the saturation magnetization, are discontinuous. For the mathematical analysis, however, it is convenient to work with parameters that are smooth functions of the position, which vary rapidly (but smoothly) at the interface between different magnets. This smoothness allows us to apply safely the standard rules of calculus (integration by parts). We obtain the case of sharp interfaces as a limit, making the parameters dependent on one additional regularizing parameter, δ, in such a way that they are smooth for $\delta > 0$ and become discontinuous at some given surface (the interface) in the limit $\delta \to 0$.

The effective field, obtained from the functional derivative of the energy with respect to $\hat{n}$, can be written as $\vec{B}_{\text{eff}} = \vec{B}^{(d)}_{\text{eff}} + \vec{B}^{(0)}_{\text{eff}}$, where $\vec{B}^{(0)}_{\text{eff}}$ does not depend on the

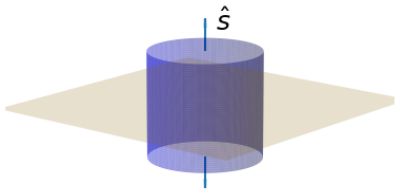

FIG. 1. A small cylindric pillbox enclosing a surface element of the interface, with the axis oriented along the normal of the surface element, $\hat{s}$.

derivatives of $\hat{n}$ and

$$\vec{B}^{(d)}_{\rm eff} = \frac{1}{M_s}\sum_i \Big(\partial_i(2A\partial_i\hat{n}) - D_i\hat{x}_i\times\partial_i\hat{n} - \hat{x}_i\times\partial_i(D_i\hat{n})\Big). \tag{2}$$

In the above equation M_s is the saturation magnetization, which is a smooth function of the position which may become discontinuous at the interface for $\delta\to 0$.

In the limit of a sharp interface ($\delta\to 0$) the magnetization may become a non smooth function which, nevertheless, has to fullfill some conditions which are derived from the structure of the Landau-Lifschitz-Gilbert (LLG) equation, which has the form

$$\partial_t\hat{n} = \gamma\vec{B}_{\rm eff}\times\hat{n} + \alpha\hat{n}\times\partial_t\hat{n}, \tag{3}$$

where $\gamma>0$ is the absolute value of the electron giromagnetic ratio and α is the Gilbert damping parameter. Using the product rule for derivatives, the term $\vec{B}^{(d)}_{\rm eff}\times\hat{n}$ can be written as

$$\vec{B}^{(d)}_{\rm eff}\times\hat{n} = \frac{1}{M_s}\sum_i\Big[\partial_i\Big((2A\partial_i\hat{n} - D_i\hat{x}_i\times\hat{n})\times\hat{n}\Big) + D_i\Big((\hat{x}_i\times\hat{n})\times\partial_i\hat{n} - (\hat{x}_i\times\partial_i\hat{n})\times\hat{n}\Big)\Big]. \tag{4}$$

To find the conditions at the interface, we consider a small cylindric pillbox which encloses a surface element of the interface, and whose axis is oriented along the normal vector of the surface element, $\hat{s}$, as in Fig. 1. The pillbox occupies the volume Ω_p and is bounded by the surface $\partial\Omega_p$. We multiply both sides of the LLG equation by M_s and integrate over Ω_p. Using the divergence theorem for the first term of the right hand side of equation (4), we get

$$\int_{\Omega_p} M_s\partial_t\hat{n}\,d^3r = \gamma\int_{\partial\Omega_p} d\sigma\sum_i\sigma_i(2A\partial_i\hat{n} - D_i\hat{x}_i\times\hat{n})\times\hat{n} + \int_{\Omega_p}\gamma\left[\sum_i D_i\Big((\hat{x}_i\times\hat{n})\times\partial_i\hat{n} - (\hat{x}_i\times\partial_i\hat{n})\times\hat{n}\Big)\right]d^3r + \int_{\Omega_p} M_s\left[\gamma\vec{B}^{(0)}_{\rm eff}\times\hat{n} + \alpha\hat{n}\times\partial_t\hat{n}\right]d^3r, \tag{5}$$

where $\hat{\sigma}$ is the normal vector of $\partial\Omega_p$. Now, we take the limit of sharp interface, $\delta\to 0$, making the following assumptions: 1) $\hat{n}$ remains continuous at all points, including the interface; 2) the derivatives $\partial_i\hat{n}$, $\partial_t\hat{n}$ remain bounded, although $\partial_i\hat{n}$ may be discontinuous at the interface. Next, we take the limit in which the pillbox thinkness tends to zero. In this limit the volume integrals and the surface integral over the curved face of the pillbox vanish, and thus equation (5) requires that

$$\vec{C} = 2A(\hat{s}\cdot\nabla)\hat{n} - (\tilde{D}\hat{s})\times\hat{n} \tag{6}$$

be continuous at the interface. Here $\tilde{D}$ is the diagonal 3×3 matrix with D_1, D_2, and D_3 in the diagonal. Continuity, obviously, means that

$$\lim_{t\to 0^+}\vec{C}(\vec{x}-t\hat{s}) = \lim_{t\to 0^+}\vec{C}(\vec{x}+t\hat{s}) \tag{7}$$

for any $\vec{x}$ at the interface. A consequence of this fact is that if A or D are discontinuous at the interface, then the derivative of $\hat{n}$ along the surface normal has to be discontinuous at the interface.

For a cubic chiral magnet $D_1=D_2=D_3=D$ and then

$$\vec{C} = 2A(\hat{s}\cdot\nabla)\hat{n} - D\hat{s}\times\hat{n}, \tag{8}$$

while for a monoaxial chiral magnet with chiral axis along $\hat{z}$ we have $D_1=D_2=0$, $D_3=D$, and then

$$\vec{C} = 2A(\hat{s}\cdot\nabla)\hat{n} - D(\hat{z}\cdot\hat{s})\hat{z}\times\hat{n}. \tag{9}$$

If the magnet is in contact with a non magnetic medium (vacuum or air, for instance), then $\vec{C}$ has to vanish at the boundary, because it vanishes in the non magnetic medium, since there A and D vanish. This is the boundary condition which originates the well known surface chiral twists.

On the other hand, if a magnet (chiral or not) is in contact with a very hard magnet, the expression (7) has to be equated to $A_h(\hat{s}\cdot\nabla)\hat{n}$, which corresponds to the hard magnet side. If the stiffness constant of the hard magnet, A_h, is very large, then $(\hat{s}\cdot\nabla)\hat{n}$ has to be proportionally small on the hard magnet side, and it vanishes in the limit $A_h\to\infty$. In this limit $\hat{n}$ has direction of the equilibrium magnetization of the hard magnet and equation (7) is continuous because on the hard magnet part $A_h(\hat{s}\cdot\nabla)\hat{n}$ can take any value. We obtain in this way Dirichlet boundary conditions.

As a word of caution, let us notice that the discussion on conditions at interfaces presented here, including boundary conditions, ignores the possible existence of surface anisotropies, in which case the condition at the interface would be

$$\lim_{t\to 0^+}\Big(\vec{C}(\vec{x}+t\hat{s}) - \vec{C}(\vec{x}-t\hat{s})\Big) = \vec{S}, \tag{10}$$

where $\vec{S}$ is the contribution of the surface anisotropy to the volume integrals of (5), which does not vanish in the limit of sharp interface ($\delta\to 0$) and infinitely thin pillbox,

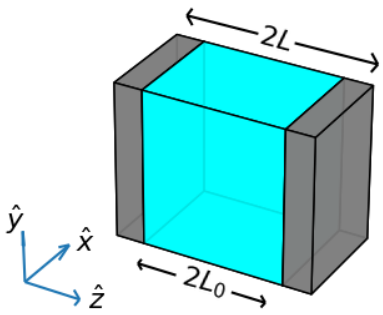

FIG. 2. Composite magnet. The cyan region is occupied by a monoaxial chiral magnet and the gray regions by two similar slabs of a uniaxial ferromagnet. The chiral axis is oriented along the $\hat{z}$ direction.

in this order. Hence, $\vec{C}$ could be discontinuous at the interface.

Finally, it is worthwhile to stress that at a sharp interface that separates two magnetic media the saturation magnetization becomes discontinuous, what induces a surface density of magnetic charge at each point $\vec{x}$ of the surface, given by

$$\lim_{t\to 0^+} \Big(M_s(\vec{x}-t\hat{s}) - M_s(\vec{x}+t\hat{s})\Big)\hat{s}\cdot\hat{n}. \tag{11}$$

This surface magnetic charge contributes to the magnetostatic field of the two media, but does not affect the interface conditions given by (7) or (10) [39].

III. A COMPOSITE MAGNETIC SYSTEM

In this work, we consider a magnetic system of rectangular parallelepiped shape which occupies a region of size $2L$ along the $\hat{z}$ direction, so that $-L \le z \le L$ (the convention for the coordinate system is described at the beginning of section II). The dimensions of the system in the directions $\hat{x}$ and $\hat{y}$ are very large and thus are considered infinite. The system is inhomogeneous along the $\hat{z}$ direction and consists of three homogeneous parts: one monoaxial chiral magnet occupies a central region of size $2L_0$, that is, the region $-L_0 \le z \le L_0$; the peripheral regions, $-L \le z < -L_0$ and $L_0 < z \le L$, are occupied by two similar uniaxial ferromagnets, as in figure 2. The materials are oriented so that the chiral axis of the monoaxial chiral magnet is aligned with the $\hat{z}$ axis, and the easy axis of each ferromagnet is aligned with the $\hat{x}$ axis. The direction of the magnetization is given by the unit vector field $\hat{n}$.

It is convenient to introduce the characteristic functions $\chi_c(z)$ and $\chi_u(z)$, defined by $\chi_c(z) = 1$ if $|z| \le L_0$ and $\chi_c(z) = 0$ otherwise, and by $\chi_u(z) = 1$ if $L_0 < |z| \le L$ and $\chi_u(z) = 0$ otherwise. The energy of the system is given by

$$E = \int d^3r\, (\chi_c W_c + \chi_u W_u), \tag{12}$$

where W_c and W_u are the energy densities of the monoaxial chiral magnet and of the uniaxial ferromagnet, respectively, and have the form

$$W_c = A\sum_i \partial_i\hat{n}\cdot\partial_i\hat{n} - D\hat{z}\cdot(\hat{n}\times\partial_z\hat{n}) - K_c(\hat{z}\cdot\hat{n})^2, \tag{13}$$

$$W_u = \rho A\sum_i \partial_i\hat{n}\cdot\partial_i\hat{n} - K_u(\hat{x}\cdot\hat{n})^2. \tag{14}$$

In the above expressions A is the stiffeness constant of the chiral magnet and the dimensionless parameter ρ is the ratio beween the stiffness constants of the ferromagnet and the chiral magnet. The chiral magnet has a uniaxial anisotropy, which is of easy-plane type, whose axis coincides with the chiral axis $\hat{z}$, and whose energy per unit volume is given by the anisotropy constant $K_c < 0$. The ferromagnet has its easy axis along $\hat{x}$ and its anisotropy constant is $K_u > 0$. Finally, D sets the strength of the DMI interaction in the chiral magnet. We ignore the magnetostatic energy since it can be included in the anisotropies for the one dimensional modulations considered in this work [41]. Notice also that we consider only the case of zero applied field.

The effective field is given by $\vec{B}_{\rm eff} = -(1/M_s)\delta E/\delta\hat{n}$, where the saturation magnetization M_s is a function of z given by $M_s(z) = M_c\chi_c(z) + M_u\chi_u(z)$, and M_c and M_u are the saturation magnetizations of the chiral magnet and the ferromagnet, respectively. If $\hat{n}$ satisfies the conditions discussed in section II, that is, continuity of $\hat{n}$ and $\vec{C}$, integration by parts can be applied to obtain the functional derivative in the standard way, and we obtain $\vec{B}_{\rm eff} = (2A/M_s)\vec{b}_{\rm eff}$, where

$$\begin{aligned}\vec{b}_{\rm eff} = a\nabla_T^2\hat{n} + \partial_z\big(a\partial_z\hat{n} - q_0\chi_c\hat{z}\times\hat{n}\big) - q_0\chi_c\hat{z}\times\partial_z\hat{n} \\ + q_0^2\kappa\chi_c(\hat{z}\cdot\hat{n})\hat{z} + \rho q_u^2\chi_u(\hat{x}\cdot\hat{n})\hat{x}.\end{aligned} \tag{15}$$

In the above expresion we introduced $\nabla_T^2 = \partial_x^2 + \partial_y^2$,

$$q_0^2 = \frac{D}{2A}, \quad \kappa = \frac{AK_c}{D^2}, \quad q_u^2 = \frac{K_u}{\rho A}, \tag{16}$$

and the function $a(z) = \chi_c(z) + \rho\chi_u(z)$.

At the interfaces $z = \pm L_0$, both $\hat{n}$ and $\vec{C}$, given by (9) with $\hat{s} = \hat{z}$, have to be continuous. The condition of continuity of $\vec{C}$ at $z = L_0$ can be cast to the form

$$\lim_{z\to L_0^-}\big(\partial_z\hat{n} - q_0\hat{z}\times\hat{n}\big) = \lim_{z\to L_0^+}\rho\,\partial_z\hat{n}. \tag{17}$$

An analogous condition holds for $z = -L_0$. We call these conditions at $z = \pm L_0$ the *matching conditions*.

Finally, the ferromagnetic slabs are in contact at $\pm L$ with a non magnetic medium, what means that expression (7), with $\hat{s} = \hat{z}$ and $\tilde{D} = 0$, has to vanish at the boundaries $z = \pm L$. This provides the Neumann boundary conditions

$$\partial_z\hat{n}(-L) = \partial_z\hat{n}(L) = 0. \tag{18}$$

IV. HELICAL STATES

Since we seak static magnetic states with modulations only along the $\hat{z}$ direction, the effective field can be written as

$$\vec{b}_{\rm eff} = \begin{cases} \hat{n}'' - 2q_0\hat{z}\times\hat{n}' + q_0^2\kappa(\hat{z}\cdot\hat{n})\hat{z}, & |z|<L_0, \\ \rho\big(\hat{n}'' + q_u^2(\hat{x}\cdot\hat{n})\hat{x}\big), & L_0<|z|<L, \end{cases} \tag{19}$$

where the prime means derivative with respect to z.

The equation for the static states is $\vec{b}_{\rm eff}\times\hat{n}=0$. Equation (19) implies that we have to solve one differential equation for $|z|<L_0$ and another one for $L_0<|z|<L$, and to impose the matching condition (17) at $z=L_0$ and the analogous condition for $z=-L_0$, and the boundary conditions (18).

The static equations admit solutions in which the magnetization lies on the easy plane of the chiral magnet, and thus can be written as

$$\hat{n} = \cos\varphi\,\hat{x} + \sin\varphi\,\hat{y}, \tag{20}$$

where the function $\varphi(z)$ is a solution of

$$\varphi'' = 0, \quad |z|<L_0, \tag{21}$$

$$\varphi'' - q_u^2\sin\varphi\cos\varphi = 0, \quad L_0<|z|<L, \tag{22}$$

which satisfies the boundary conditions and the matching conditions. We proof in the next subsections that there exist a big number of such solutions.

The idea is as follows. The general solution of (21) is $\varphi(z) = C + pq_0 z$, where C and p are arbitrary constants, while equation (22) is the well known double Sine-Gordon equation, which also has a known two parameter family of solutions. This allows us to construct exact solutions for the whole system, which satisfy the differential equations (21) and (22), the boundary conditions, and the matching conditions.

Let $\varphi_{\rm sg}(z,A,B)$ the two-parameter family of solutions of equation (22), where A and B are the parameters (see appendix A). We build a solution of the whole system as

$$\varphi(z) = \begin{cases} \varphi_{\rm sg}(z,A_1,B_1), & -L<z<-L_0, \\ C+pq_0z, & -L_0<z<L_0, \\ \varphi_{\rm sg}(z,A_2,B_2), & L_o<z<L, \end{cases} \tag{23}$$

We have to impose the boundary and the matching conditions, which are six conditions. Since we have six free parameters, A_1, B_1, A_2, B_2, C, and p, we should expect generically that the value of p will be fixed by these conditions. However, as we show in the remaining of this section, the fact that the magnetic state is of helical nature within the chiral magnet implies that the matching conditions have an oscillatory character and there are many solutions for p, its number growing linearly with the size of the chiral magnet, L_0.

A. Explicit form of the solution

Specifically, we propose a symmetric solution which has helical nature within the chiral magnet, given by

$$\varphi(z) = \begin{cases} -\sigma_p\,\varphi_0(-z), & -L<z<-L_0, \\ pq_0z, & -L_0<z<L_0, \\ \sigma_p\,\varphi_0(z), & L_o<z<L, \end{cases} \tag{24}$$

where the parameter p, which is the helix wave number in units of q_0, is to be determined. In equation (24) we introduce $\sigma_p=1$ if $p\geq 1$ and $\sigma_p=-1$ if $p<1$. As it will become clear in the following, σ_p is needed to satisfy the matching conditions (17). The function $\varphi_0(z)$ is the solution of equation (22) with $-\pi<\varphi_0<0$ and

$$\varphi_0(z_0) = -\frac{\pi}{2}, \quad \varphi_0'(L)=0, \quad \varphi_0'(z)>0, \tag{25}$$

where $z_0<L$ is a point to be determined by imposing the matching conditions. The explicit form of φ_0 is obtained in appendix A, and is given by

$$\varphi_0(z) = -\arccos\Big(\eta\,{\rm sn}\big(q_u(z-z_0),\eta\big)\Big), \tag{26}$$

where ${\rm sn}(x,\eta)$ is the Jacobi elliptic function, with ellipticity modulus η, and $z_0<L$ is chosen such that $\varphi_0(z_0)=-\pi/2$. If $L-L_0$ is large, we may visualize φ_0 as a domain wall centered at z_0, which connects two domains with magnetization pointing along $\pm\hat{x}$ for $z\to\pm\infty$.

Equation (26) is complemented with

$$K(\eta) = q_u(L-z_0), \tag{27}$$

where $K(\eta)$ is the complete elliptic integral of the first kind. The above equation, which determines the parameter η, ensures that the boundary condition $\varphi'(L)=0$ is satisfied (see appendix A). Taking into account that ${\rm sn}\big(K(\eta),\eta\big)=1$, equation (26) gives $\eta=\cos\varphi_0(L)$.

Summarizing, the magnetic state given by (24) consists of a helical state of wave number pq_0 within the chiral magnet connected at $z=L_0$ to a section of a domain wall hosted by the ferromagnet in the $z>L_0$ region. The wall center, z_0, is a free parameter tuned to enforce the matching conditions. The helical state is also connected to a section of another domain wall section hosted by the ferromagnet in the $z<-L_0$ region. This latter domain wall is obtained from the former domain wall by a symmetry. The domain wall center, z_0, need not be at a physical point inside the ferromagnetic slab, but can lie in the region $z<L_0$. Actually, this view of the magnetic states in the ferromagnetic slabs as sections of domain walls holds only if the slabs are thick enough. However, we find it useful to think of these magnetic states as domain walls.

B. Matching conditions

The matching conditions select the possible values of p. The continuity of $\hat{n}(z)$ is guaranteed if and only if

$$\cos\varphi_0(L_0) = \cos(pq_0L_0), \tag{28}$$

$$\sigma_p \sin\varphi_0(L_0) = \sin(pq_0L_0), \tag{29}$$

that is

$$\sigma_p\varphi_0(L_0) = (pq_0L_0) \bmod 2\pi. \tag{30}$$

The matching condition (17) reduces to

$$\rho\sigma_p\varphi_0'(L_0) = (p-1)q_0, \tag{31}$$

which, taking into account the form of φ_0' (appendix A), the definition of σ_p, and equation (28), can be cast to the form

$$|p-1| = \frac{\rho q_u}{q_0}\sqrt{\eta^2 - \cos^2(pq_0L_0)}. \tag{32}$$

By symmetry, the matching condition at $z=-L_0$ is also satisfied if equation (32) holds.

Equations (27), (30), and (32) determine completely the magnetic states of the form (24). They constitute a system of three equations with three unknowns: η, z_0, and p. Since $0 \le \eta < 1$, the right hand side of (32) is bounded by $\rho q_u/q_0$, what implies the following bounds for p:

$$1 - \frac{\rho q_u}{q_0} \le p \le 1 + \frac{\rho q_u}{q_0}. \tag{33}$$

C. The number of p states

We show here that equations (27), (30), and (32), which determine the p states, have many solutions, with different values of p, and that the number of solutions increases proportionally to the size of the chiral magnet, L_0. We provide below an argument that shows that this statement is true if L_0 and $L-L_0$ are large. The numerical solution of the system of equations indicates that it is also true if $L-L_0$ is not large. Therefore, we conclude that there are many states of the form (24) differing by the wave number pq_0 of the helical part (the magnetization of the ferromagnetic slabs is also different for different values of p, of course). The values of p for these states become dense in a certain interval $p_{\min} < p < p_{\max}$ in the limit $L_0 \to \infty$ (but $L-L_0$ may remain finite).

Let us argue in the large $L-L_0$ limit, in which the analysis is considerably simplified. To work in this limit it is convenient to substitute the ellipticity modulus η by the *nome*, defined by $q = \exp\big(-\pi K/\bar{K}\big)$, where [42]

$$K = K(\eta), \quad \bar{K} = K\big(\sqrt{1-\eta^2}\big). \tag{34}$$

Hence, from now on we consider that η is a function of q, given by inverting the equation that defines the nome. Notice that equation (27) means that the nome is exponentially small, $q \sim \exp\big(-2q_u(L-L_0)\big)$, for large $L-L_0$. Using the properties of the complete elliptic integral K [43], we see that $\eta = 1+O(q)$ and then equation (32) has the form

$$p - 1 = -\frac{\rho q_u}{q_0}\,\sin(pq_0L_0) + O(q^b), \tag{35}$$

where $b = 1/2$ if $\sin(pq_0L_0) = 0$ and $b = 1$ otherwise. Also, using $\mathrm{sn}(x,\eta) = \tanh x + O(q)$, we obtain that for large $L - L_0$

$$\varphi_0(z) = -2\,\mathrm{atan}\,\mathrm{e}^{-q_u(z-z_0)} + O(q). \tag{36}$$

Thus, as we said before, φ_0 has the form of a conventional domain wall centered at z_0, with some correction exponentially small with L.

Finally, combining equations (36) and (30) we get

$$\tanh\big(q_u(L_0 - z_0)\big) = \cos(pq_0L_0) + O(q). \tag{37}$$

This gives an explicit solution for z_0 if we neglect the $O(q)$ term.

It is clear that equation (35) has many solutions if we neglect the $O(q)$ term, and it is also clear that this term, exponentially small with $L-L_0$, cannot change this behavior. Moreover, it is also clear that the number of solutions increases proportionally to q_0L_0, and thus the values of p that solve equation (35), or equation (32), become dense in the interval (33) in the limit $L_0 \to \infty$. Thus, there is a continuum of helical states in the limit $q_0L_0 \to \infty$, as claimed in reference 35. Figure 3 illustrates these statements.

D. Energy of the p states

The energy density (total energy divided by $2L$) can be readily computed and has the form

$$e(p) = Aq_0^2\frac{L_0}{L}\Big(e_c(p) + e_u(p)\Big), \tag{38}$$

where $e_c(p) = (p-1)^2 - 1$ is the energy density of the helical state within the chiral magnet, which is independent of its size L_0, and $e_u(p)$ is the contibution of the ferromagnetic slabs, which has the form

$$e_u(p) = \frac{\rho\eta^2}{q_0L_0}\frac{q_u}{q_0}\int_{K-x_L}^{K}\Big(1 - 2\,\mathrm{sn}^2(x,\eta)\Big)dx, \tag{39}$$

where $x_L = q_u(L-L_0)$ is the width of the slabs in units of $1/q_u$. If the slab width is kept constant, $e_u(p)$ vanishes in the large q_0L_0 limit, and the energy density of the p states attains the energy density of the chiral magnet part, $e(p) \to e_c(p)$.

The behaviour of the energy of the p states as q_0L_0 increases is interesting and will be analyzed, in some examples, in section VI. For large q_0L_0 the energy density has its minimum at $p=1$, and thus all the p states with $p \neq 1$, are at most metastable. It remains to see which, if any, of the p states are actually metastable. This problem is addressed in section V.

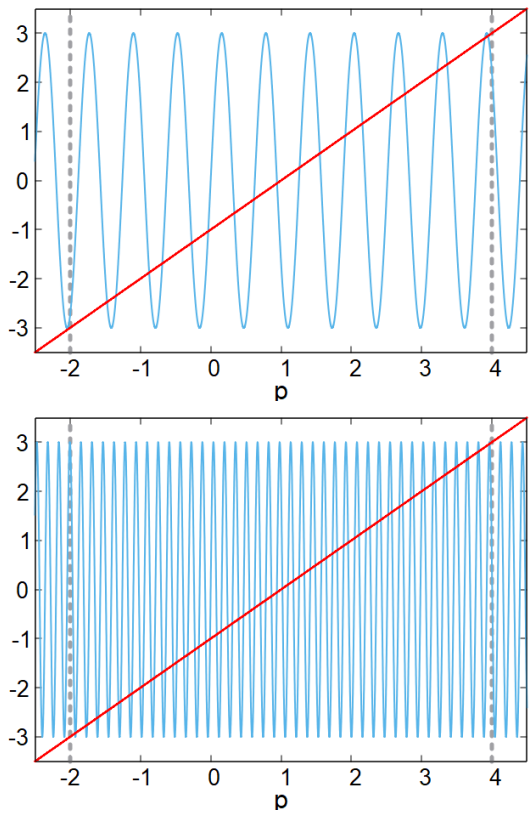

FIG. 3. Graphical illustration of the solutions of equation (35). The red line is the left-hand side of the equation, and the violet line if the right-hand side. The upper panel corresponds to $q_0 L_0 = 10$ and the lower panel to $q_0 L_0 = 40$. In both cases $\rho q_u / q_0 = 3$. The vertical dashed lines signal the bounds (33).

E. A classification of the p states

Before closing this section we notice an interesting fact about the solutions of equation (32). The derivative with respect to p of the right-hand side of equation (32) is

$$-\rho q_u L_0 \frac{\sin(pq_0L_0)\cos(pq_0L_0)}{\sqrt{\eta^2 - \cos^2(pq_0L_0)}}. \tag{40}$$

Since the sign of $\sin(pq_0L_0)$ is fixed by σ_p, see equation (29), the sign of the above expression is determined by $\cos(pq_0L_0)$. It is clear from Fig. 3 that the solutions of equation (32) correspond alternatively to points in which the right hand side of equation (32) increases and decreases. These means that $\cos(pq_0L_0)$ is positive for one half of the p's and negative for the other one half. Then, equation (37) implies that one half of the p values correspond to $z_0 < L_0$ and the other one half to $z_0 > L_0$. In the case $z_0 < L_0$ the center of the wall is outside the physical region occupied by the ferromagnetic slab, while if $z_0 > L_0$ it is within the slab. To lighten the writing, let us call the former case a *virtual* domain wall and the latter a *real* domain wall. Hence, half of the p correspond to virtual domain walls and the other half to real domain walls. We will see in next section that, if $L - L_0$ is large, all p states with real domain wall are unstable and that the p states with a virtual domain wall are stable if $p_{\min} < p < p_{\max}$, with

$$\begin{aligned} p_{\min} &= \max\left\{1 - \sqrt{h_c},\, 1 - \frac{\rho q_u}{q_0}\right\}, \\ p_{\max} &= \min\left\{1 + \sqrt{h_c},\, 1 + \frac{\rho q_u}{q_0}\right\}, \end{aligned} \tag{41}$$

where $h_c = 1 - \kappa > 1$ is the dimensionless critical field of the chiral magnet.

The case $p = 1$ is somehow especial. In this case equations (30) and (31) give $\cos(\varphi_0(L_0)) = \pm\eta$. Then, from equation (A6), we get $\mathrm{sn}(x_0, \eta) = \pm 1$, where $x_0 = q_u(L_0 - z_0)$. The solution for the plus case is $x_0 = K(\eta)$, which, on account of (27), is only possible if $L_0 = L$, that is, if the thickness of the ferromagnetic slabs vanishes. So, this possibility is realized only if the system consists of a monoaxial chiral magnet in contact with a nonmagnetic material. For the minus case we have $x_0 = -K$, and this gives $z_0 = (L_0 + L)/2$. This means the center of the wall is in the middle of the ferromagnetic slab, hence it is a real wall, and therefore unstable. In spite of this discussion, $p = 1$ can also be realized if the chiral magnet is in contact with ferromagnetic slabs, in the sense that we can get metastable states with p as close to 1 as wanted by making $q_0 L_0$ sufficiently large.

V. STABILITY OF THE HELICAL STATES

To be useful, the p states have to be metastable, that is, they have to be local minima of the energy. Let $\hat{n}_p$ be the magnetization of the p state, given by equation (20), with φ given by (24). A necessary condition for the p state to be a local minimum of the energy is the positivity of the second variation of the energy, $\delta^{(2)}E$, at $\hat{n}_p$. Thus, the analysis of $\delta^{(2)}E$ allows us to select the metastable p states among all those found by the procedure of the previous section.

To analyze the stability of the p state we ignore the magnetostatic energy, which cannot contribute to destabilize the p state. This is due to the fact that the magnetostatic field created by the p state vanishes, since its sources vanish: $\nabla \cdot \hat{n}_p = 0$ and $\hat{z} \cdot \hat{n}_p = 0$. Then, the magnetostatic energy of the p state is zero and, since it cannot be negative, a perturbation can only increase it.

The argument of the previous paragraph relies on the fact that we consider a system which is infinite in the directions perpendicular to the chiral axis ($\hat{x}$ and $\hat{y}$). In a real system with finite but very large dimensions along $\hat{x}$ and $\hat{y}$, the magnetostatic energy of the p states is not zero due to the magnetic poles on the surfaces perpendicular to $\hat{x}$ and $\hat{y}$. In the chiral magnet section the poles on each surface are alternatively positive and negative, due to the helical character of the magnetization, and

thus the magnetostatic energy will not be large. The effect of magnetostatice energy on the modulated states of monoaxial ferromagnets is studied in reference 21, where it is concluded that it is only relevant in the case of thin films, although some distortion of the magnetization may be expected near the surface to optimize the magnetostatic energy. If the ferromagnetic slabs are very thin, with thickness of the order of the domain wall width, the contribution of its surface magnetic poles will be negligible. If the slabs are thick, but the thickness is much smaller than the dimension of the system along the $\hat{x}$ direction, there will be a single domain in the slab, since the domain width in a uniaxial ferromagnet is proportional to its size along the easy axis [44]. Again, some distortion of the magnetization may be expected near the slab surfaces (there might even be domain branching), to optimize the magnetostatic energy. In conclusion, we expect that the results of this section will hold in a magnet large enough in the directions perpendicular to the chiral axis.

The second variation of the energy can be written in terms of two linear selfadjoint operators, K_{11} and K_{22} [*cf.* equation (44)]. The positivity of $\delta^{(2)}E$ is equivalent to the positivity of these two operators. The p state with minimum energy, which has p close to 1, is stable. We call it the equilibrium p state. For this state K_{11} and K_{22} have to be positive, what means that their spectrums lie on the positive real axis. In the infinite system studied in reference 35 the lower edge of the spectrum is continuous as a function of p, and then there is a certain interval around $p = 1$ in which the p states are metastable. We show in this section that also in the finite system there are many metastable p states, the number of which grows linearly with the size of the chiral magnet, L_0.

The existence of metastable helical states with very close values of the wave number raises a question: why a helical state which has a wave number very close to the equilibrium wave number cannot reduce its energy by changing its wave number? The answer is that, in spite of appearances, two states with very close but different wave numbers are not close in the space of magnetic configurations. In a sense, they are orthogonal, and one cannot be transformed into the other by a small perturbation, no matter how close the wave numbers are [35].

The remaining of this section is devoted to find the conditions under which K_{11} and K_{22} are positive, and to establish the conditions under which the p states satisfy these conditions. The reader not interested in the mathematical details can skip the remaining of this section and go directly to section VI, where the results are discussed.

A. The second variation of the energy

To obtain $\delta^{(2)}E$ we consider a perturbation of $\hat{n}_p$, which if it is small enough can be written in terms of two fields ξ_1 and ξ_2 as

$$\hat{n} = \sqrt{1-\xi_1^2-\xi_2^2}\,\hat{n}_p + \xi_1\,\hat{e}_1 + \xi_2\,\hat{e}_2, \tag{42}$$

where we introduce the unit vector fields

$$\hat{e}_1 = -\hat{z}, \quad \hat{e}_2 = -\sin\varphi(z)\,\hat{x} + \cos\varphi(z)\,\hat{y}, \tag{43}$$

so that $\{\hat{e}_1, \hat{e}_2, \hat{n}_p\}$ is a right-handed orthonormal triad. To have perturbations of finite energy we restric the fields ξ_i, for $i = 1, 2$, to square integrable functions. The continuity of $\hat{n}$ and the matching conditions at $z = \pm L_0$ provide further conditions for ξ_i and $\partial_z\xi_i$, to be discussed below.

The second variation of the energy at $\hat{n}_p$ can be obtained by inserting the above perturbation into the energy functional and expanding in powers of ξ_1 and ξ_2 to the second order. A straightforward computation gives

$$\delta^{(2)}E = 2A\int d^3r\,\Big(\xi_1 K_{11}\xi_1 + \xi_2 K_{22}\xi_2\Big), \tag{44}$$

where K_{11} and K_{22} are linear differential operators defined by their action on functions ξ as

$$K_{ii}\,\xi = -a\nabla_T^2\xi - \partial_z(a\partial_z\xi) + Q_{ii}\,\xi, \quad i = 1, 2, \tag{45}$$

where

$$Q_{11} = q_0^2\Big(h_c - (p-1)^2\Big)\chi_c + \rho\big(q_u^2\eta^2 - 2\varphi'^2\big)\chi_u, \tag{46}$$

$$Q_{22} = \rho\Big(q_u^2\eta^2 - 2\varphi'^2 - \rho q_u^2(1-\eta^2)\Big)\,\chi_u, \tag{47}$$

and where, we recall, $h_c = 1 - \kappa > 1$ and $a(z) = \chi_c(z) + \rho\chi_u(z)$ is the function defined at the end of section III.

The positivity of $\delta^{(2)}E$ is equivalent to the positivity of K_{11} and K_{22}. These operators are selfadjoint in an appropriate domain, and they are positive if and only if their spectrum lies on the positive real axis.

B. The operators K_{11} and K_{22}

Since the "potentials" Q_{11} and Q_{22} depend only on z, to study the spectrum of K_{11} and K_{22} it is convenient to perform the Fourier transform in the coordinates x and y. To avoid symbol proliferation we use the same notation for functions and operators in the real and transformed space. After the Fourier transformation we have

$$K_{ii}\,\xi = -\big(a\xi'\big)' + ak_T^2\xi + Q_{ii}\,\xi. \tag{48}$$

Now ξ is a function of the Fourier wave vector $\vec{k}_T = k_x\hat{x} + k_y\hat{y}$, and of z, and the prime means derivative with respect to z.

The continuity of $\hat{n}$ and the matching conditions (17) imply that ξ and $a\xi'$ have to be continuous (here ξ represents either ξ_1 or ξ_2). In particular, the matching condition implies

$$\lim_{z\to L_0^-}\xi'(z) = \lim_{z\to L_0^+}\rho\,\xi'(z). \tag{49}$$

An analogous relation holds for $z \to -L_0^{\pm}$. Finally, the boundary conditions for $\hat{n}$ give

$$\xi'(-L) = 0, \quad \xi'(L) = 0. \tag{50}$$

After the Fourier transformation, K_{11} and K_{22} are particular cases of a general kind of differential operators thoroughly studied in reference 45. Their actions are well defined on continuous functions ξ defined in $[-L, L]$, which are piecewise continuously differentiable and such that $a\,\xi'$ is also continuous and piecewise continuously differentiable, and satisfy the boundary conditions (50) [46]. The operators are selfadjoint in the appropiate extended domain and have a purely discrete [45].

The eigenvalues of K_{ii} are given by the values of λ for which the differential equation

$$K_{ii}\xi = \lambda\xi \tag{51}$$

has solutions which satisfy the matching conditions (49) and the boundary conditions (50). A necessary condition for the stability of the p state is that the eigenvaules of K_{11} and K_{22} be positive.

C. Bounds on the spectrum

The spectrum of operators like K_{11} and K_{22} is bounded from below, since Q_{11} and Q_{22} are functions bounded from below. Indeed, multiplying equation (51) by ξ, integrating from $[-L, L]$, and then using integration by parts and the boundary conditions (50), the following bound for the spectrum of K_{22} is obtained:

$$\lambda \geq \min\left\{\rho(k_T^2 - q_u^2), 0\right\}. \tag{52}$$

Similarly, for the spectrum of K_{11} we get the bound

$$\lambda \geq \min\left\{k_T^2 + \left[h_c - (p-1)^2\right]q_0^2, \;\; \rho(k_T^2 - q_u^2\eta^2)\right\}. \tag{53}$$

D. Eigenvalue equations

To study the spectrum of K_{11} and K_{22} it is convenient to introduce the quantities

$$\beta_1 = \eta^2 + \frac{k_T^2 - \lambda/\rho}{q_u^2}, \quad \beta_2 = 2\eta^2 - 1 + \frac{k_T^2 - \lambda/\rho}{q_u^2}, \tag{54}$$

$$\gamma_1 = h_c - (p-1)^2 + \frac{k_T^2}{q_0^2} + \frac{\rho q_u^2}{q_0^2}\left(\beta_1 - \eta^2 - \frac{k_T^2}{q_u^2}\right), \tag{55}$$

$$\gamma_2 = \frac{k_T^2}{q_0^2} + \frac{\rho q_u^2}{q_0^2}\left(\beta_2 - 2\eta^2 + 1 - \frac{k_T^2}{q_u^2}\right). \tag{56}$$

Since the operators K_{11} and K_{22} commute with the parity operator, their eigenfunctions can be chosen as even or odd functions. From the form of these operators, we see the that the eigenfunctions, u, of K_{ii}, with $i = 1, 2$, can be written, for $z \geq 0$, as

$$u(z) = c_1 v(q_0 z, \gamma_i)\chi_c(z) + c_2 w\big(x, \beta_i\big)\chi_u(z), \tag{57}$$

where $x = q_u(z - z_0)$, c_1 and c_2 are constants to be determined, $v(x, \gamma)$ is a particular, even or odd, solution of

$$v'' - \gamma v = 0, \tag{58}$$

and $w(x, \beta)$ is a particular solution of

$$w'' + \frac{2}{q_u^2}\,\varphi_0'^2\, w - \beta w = 0, \tag{59}$$

which satisfies the condition $w'\big(K, \beta\big) = 0$. Equations (58) and (59) are simply the restriction of equation (51) to $|z| < L_0$ and $L_0 < z < L$, respectively. In equation (59) we use the coordinate $x = q_u(z - z_0)$, and thus $z = L$ corresponds to $x = K$, due to equation (27). The form of the eigenfunction for $z < 0$ can be obtained from the parity symmetry. It should be clear that, in equation (59), $\varphi_0'^2$, which is given by equation (A9) of appendix A, is evaluated at $z = z_0 + x/q_u$.

We are interested only in studying the existence of non positive eigenvalues, $\lambda \leq 0$. For this case equations (52) and (53) give the bounds

$$\beta_{\min}^{(i)} \leq \beta_i \leq \beta_{\max}^{(i)}, \tag{60}$$

where

$$\beta_{\min}^{(1)} = \eta^2 + k_T^2/q_u^2, \quad \beta_{\min}^{(2)} = 2\eta^2 - 1 + k_T^2/q_u^2, \tag{61}$$

and

$$\beta_{\max}^{(1)} = \max\left\{2\eta^2, \eta^2 + \frac{\rho - 1}{\rho}\,\frac{k_T^2}{q_u^2} + \frac{q_0^2}{\rho q_u^2}\left(h_c - (p-1)^2\right)\right\}, \tag{62}$$

and $\beta_{\max}^{(2)} = 2\eta^2$.

The functions v and w entering equation (57) have to fullfill the matching conditions at $z = L_0$ (then, the parity symmetry guaranties that they are fullfilled also at $z = -L_0$). This conditions can hold non trivially (that is, with $u \neq 0$) only for specific values of β, which give the eigenvalues of the corresponding operator.

We observe that we have four matching conditions, corresponding to the even and odd eigenfunctions of K_{11} and K_{22}. We identify each condition by a pair (i, s), where $i = 1, 2$ and $s = e, o$ label the operator and the eigenfunction parity, respectively. Each matching condition sets a system of two homogeneous linear equations where the unkowns are the constants c_1 and c_2 entering equation (57). To have non trivial solutions a condition $F_i^{(s)}(\beta_i) = 0$ must hold. The four functions $F_i^{(s)}(\beta)$ are given by

$$F_i^{(s)}(\beta) = v_s'(q_0 L_0, \gamma_i)w(x_0, \beta) - \frac{\rho q_u}{q_0} v_s(q_0 L_0, \gamma_i)w'(x_0, \beta) \tag{63}$$

where $x_0 = q_u(L_0 - z_0)$. In the above equation it is understood that γ_i is computed with $\beta_i = \beta$, and $v_s(x,\gamma)$ are solutions of equation (58) with definite parity, which can be chosen as

$$\begin{aligned} &v_e(x,\gamma) = \cosh(\sqrt{\gamma}x),\ v_o(x,\gamma) = \sinh(\sqrt{\gamma}x),\ \gamma > 0,\\ &v_e(x,\gamma) = 1, \quad v_o(x,\gamma) = x, \quad \gamma = 0,\\ &v_e(x,\gamma) = \cos(\sqrt{-\gamma}x),\ v_o(x) = \sin(\sqrt{-\gamma}x),\ \gamma < 0. \end{aligned} \tag{64}$$

For given p, equations $F_i^{(s)}(\beta) = 0$ determine the eigenvalues of K_{11} and K_{22}. The p state will be stable if

$$F_i^{(s)}(\beta) \neq 0, \quad \beta_{\min}^{(i)} \leq \beta \leq \beta_{\max}^{(i)} \tag{65}$$

for $i = 1, 2$ and $s = e, o$.

E. Solution of equation (59)

It remains to find the solutions of equation (59), which is studied in appendix B. Here, we summarize the results. The solutions which satisfies the boundary condition $w'(K,\beta) = 0$ can be written as

$$w(x,\beta) = w_+(x,\alpha) + d\, w_-(x,\alpha), \tag{66}$$

where w_+ and w_- are two linearly independent solutions of equation (59) which can be expressed in terms of the Jacobi theta functions θ_1 and θ_2 as

$$w_\pm(x,\alpha) = \pm\frac{\phi_1'(0,q)}{\phi_1(\alpha,q)}\,\frac{\phi_2(x\pm\alpha,q)}{\phi_2(x,q)}\exp\left(\mp\frac{\phi_1'(\alpha,q)}{\phi_1(\alpha,q)}\,x\right) \tag{67}$$

with

$$\phi_i(x,q) = \theta_i\left(\mathrm{i}\frac{\pi x}{2\bar{K}}, q\right), \quad i = 1,2,3,4. \tag{68}$$

The nome q is defined just above equation (34). The parameter $\alpha > 0$, which has nothing to do with the Gilbert damping parameter entering the LLG equation, is related to β through the equation

$$\mathrm{sn}^2(\alpha,\eta) = \frac{1}{\beta + 1 - \eta^2}, \tag{69}$$

and the constant d is determined from the boundary condition, $w'(K,\beta) = 0$, and is given by

$$d = -\exp\left(\frac{\pi\alpha}{\bar{K}} - 2\frac{\phi_1'(\alpha,q)}{\phi_1(\alpha,q)}K\right). \tag{70}$$

Now we can introduce $w(x,\beta)$ in the eigenvalue equations (63) and analyze them numerically. However, it is useful to analyze first the limit of large $q_u(L-L_0)$, which leads to important simplifications.

F. Analysis for large $q_u(L - L_0)$

The large $q_u(L - L_0)$ regime corresponds to $q \to 0$. This limit is studied in appendix C, where the formulas used in this section are derived. There, it is observed that we have to distinguish the case $\beta > 1$ from the case $\beta = 1$, which is especial.

If β is not too close to one, the solution of equation (69) is

$$\alpha = \sqrt{\beta} + O(q), \tag{71}$$

and, taking into account that $K = -\log\sqrt{q} + O(q\log q)$, we have

$$d = -\exp\Big(2\alpha + \sqrt{\beta}\log q + O(q\log q)\Big). \tag{72}$$

Hence d is negligible for large L, which corresponds to small q. Then $w(x,\beta)$ can be approximated by $w_+(x,\alpha)$, which in its turn can be expanded in powers of q. For fixed x we obtain the simple expression

$$w(x,\beta) = \left(\sqrt{\beta} + \tanh x\right)\,\mathrm{e}^{-\sqrt{\beta}x} + O(q\log q). \tag{73}$$

Neglecting the $O(q\log q)$ terms, this is the solution we would have obtained had we considered an infinite system with $u'(x,\beta) \to 0$ for $x \to \infty$ as a boundary condition.

We now analyze $F_2^{(e)}(\beta)$ for $k_T = 0$ and large β. Using equation (73), ignoring the $O(q\log q)$ corrections, we obtain that for $\beta \to \infty$

$$F_2^{(e)}(\beta) \sim \left(1 + \frac{1}{\sqrt{\rho}}\right)\frac{\rho q_u}{q_0}\exp\Big(\sqrt{\beta}\big(\sqrt{\rho}q_u L_0 - x0\big)\Big). \tag{74}$$

Thus, $F_2^{(e)}(\beta) > 0$ for large β.

For $\beta = 1$ the solution of equation (69) has the form $\alpha = K - \bar{\alpha}$, where $\bar{\alpha}$ is of order one for $q \to 0$ (see appendix C). The leading term in q of $w(x,\beta=1)$ is given by equation (C12). From it, it is straightforward to get

$$F_2^{(e)}(1) = \big(6 + 2\sqrt{6}\big)\frac{\rho q_u}{q_0}\frac{\tanh x_0}{\cosh x_0} + O(q\log q). \tag{75}$$

Thus, $F_2^{(e)}(1) < 0$ if $x_0 < 0$. Therefore, the corresponding states are unstable because $F_2^{(e)}(\beta)$ has a zero for $\beta > 1$. Since $x_0 < 0$ means $z_0 > L_0$, we see that all p states which have a real domain wall are unstable, as claimed in section IV. These unstable states correspond to half of the solutions of equation (32).

G. Analysis of states with large p

Consider again $k_T = 0$. If $|p-1| > \sqrt{h_c}$ we have that $\gamma_1 < 0$ in a neighborhood of $\beta = 1$. Then, for β

q_0L_0	10	20	40	80	100	120	240	480	960
N_p	8	16	32	63	78	93	220	373	746
N_p/q_0L_0	0.8	0.8	0.8	0.79	0.78	0.78	0.77	0.78	0.78

TABLE I. Number of metastable states, N_p, *versus* q_0L_0 for the case of thick ferromagnetic slabs: $q_u(L-L_0)=40$. The system parameters are given at the beginning of section VI.

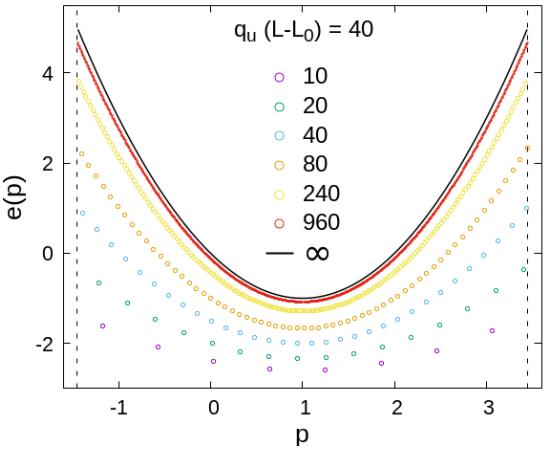

FIG. 4. Energy density of p states, in units of Aq_0^2, as a function of p in the case of thick ferromagnetic slabs, $q_u(L-L_0)=40$, for the values of q_0L_0 displayed in the legend. The system parameters are given at the beginning of section VI. The black line, labeled as ∞, corresponds to the infinite chiral magnet studied in reference 35. The vertical lines mark the limits $p_{\min}$ and $p_{\max}$ given by equation (41).

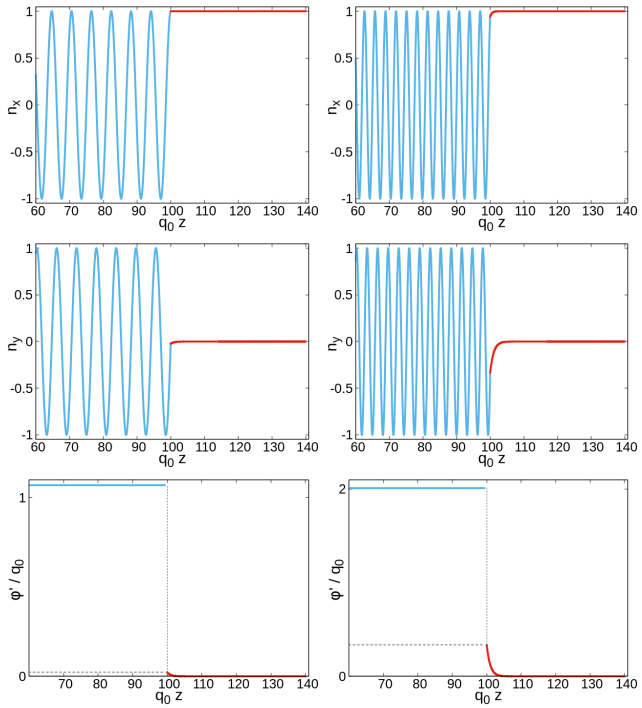

FIG. 5. Magnetization of p states in the composite magnet system for the case of thick ferromagnetic slabs, with $q_u(L-L_0)=40$. The size of the chiral magnet is $q_0L_0=100$. The system parameters are given at the beginning of section VI. From top to bottom the figures show n_x, n_y, and φ'/q_0 versus q_0z. The left panels correspond to $p=1.068$ and the right panels to $p=2.007$.

sufficiently close to one we have

$$F_1^{(e)}(\beta) = -\sqrt{-\gamma_1}\sin\left(\sqrt{-\gamma_1}q_0L_0\right)w(x_0,\beta) - \frac{\rho q_u}{q_0}\sin\left(\sqrt{-\gamma_1}q_0L_0\right)w'(x_0,\beta). \tag{76}$$

By continuity, small changes of β produce small changes on $w(x_0,\beta)$, $w'(x_0,\beta)$, and γ_1. But if q_0L_0 is large, the trigonometric functions entering the above equation suffer big oscillations, so that that $F_1^{(e)}(\beta)$ changes sign in a neighborhood of $\beta=1$. Hence, states with $|p-1|>\sqrt{h_c}$ are unstable. This relation, toghether with equation (33), provides the bounds (41).

VI. DISCUSION OF SOME RESULTS

Let us discuss the results in two cases: one in which the ferromagnetic slabs attached to the chiral magnet are thick and another one in which they are very thin. In both cases we consider $h_c=6$, $\rho=3$ and $q_u=q_0$. The possible p states are obtained by solving numerically the coupled equations (27) and (32), and their stability by evaluating numerically the functions $F_i^{(s)}(\beta)$, defined in equation (63).

A. Thick ferromagnetic slabs

We take $q_u(L-L_0)=40$, which can be considered in the large $q_u(L-L_0)$ regime, and thus we confirm by numerical means the results of section V. Recall that we say that the system has a real domain wall if the center of the wall which characterizes the magnetization in the ferromagnetic slab lies within the slab, and that it has a virtual domain wall if the center lies outside the slab. We get the following results:

1. States that have a real domain wall are unstable, whatever the value of p, in agreement with the analysis of section V F.

2. States with $|p-1|>\sqrt{h_c}$ are always unstable, in agreement with the argument of section V G.

3. States with a virtual domain wall and $|p-1|<\sqrt{h_c}$ are metastable.

4. The number of metastable p states, N_p, grows linearly with q_0L_0 (see table I), and the values of such p are homogeneously distributed in the interval $1-\sqrt{h_c}\le p\le 1+\sqrt{h_c}$. Hence, the bounds (41) are saturated.

q_0L_0	10	20	40	80	100	120	240	480	960
N_p	10	19	38	76	92	112	226	453	882
N_p/q_0L_0	1	0.95	0.95	0.95	0.92	0.93	0.94	0.94	0.92

TABLE II. Number of metastable states, N_p, *versus* q_0L_0 for the case of thin ferromagnetic slabs: $q_u(L-L_0)=1$. The system parameters are given at the beginning of section VI.

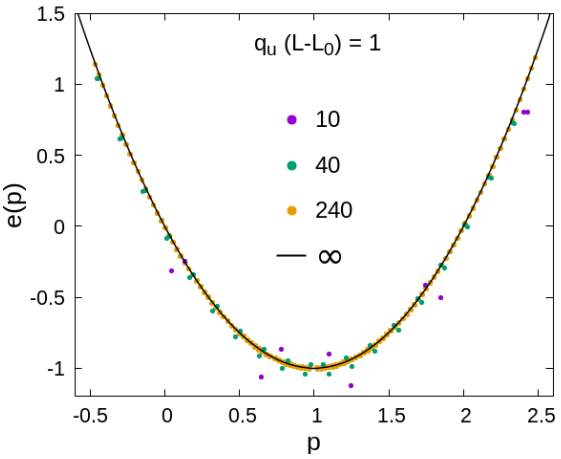

FIG. 6. Energy density of p states, in units of Aq_0^2, as a function of p in the case of thin ferromagnetic slabs, with $q_0(L-L_0)=1$, for the values of q_0L_0 displayed in the legend. The system parameters are given at the beginning of section VI. The black line, labeled as ∞, corresponds to the infinite chiral magnet studied in reference 35.

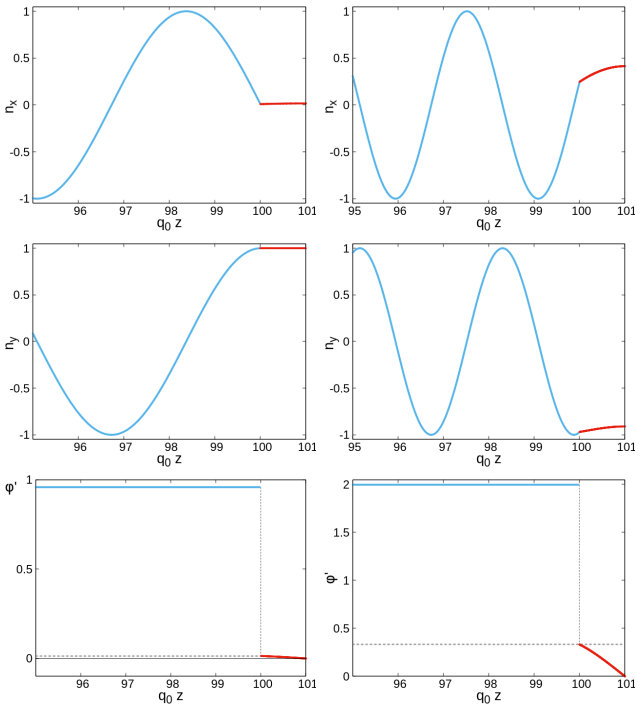

FIG. 7. Magnetization of p states in the composite magnet system for the case of thin ferromagnetic slabs, with $q_u(L-L_0)=1$. The size of the chiral magnet is $q_0L_0=100$. The system parameters are given at the beginning of section VI. From top to bottom the figures show n_x, n_y, and φ'/q_0 versus q_0z. The left panels correspond to $p=0.958$ and the right panels to $p=1.997$.

All this conclusions are in agreement with the analysis of the large $q_u(L-L_0)$ regime presented in section V F, and imply that the results of reference 35 are recoverd in the limit $q_0L_0\to\infty$.

Figure 4 shows the energy density as a function of p for different values of q_0L_0. For large q_0L_0 the convergence towards the energy density of the chiral magnet is observed (see section IV D). The composite magnet has lower energy density than the infinite chiral magnet. This is due to the fact that the magnetic state in the ferromagnetic slabs is almost uniform (it is a virtual domain wall), and the anisotropy energy contributes to lowering the system energy. Observe however that the different sets of points in figure 4 correspond to different systems and the comparison of energies has no clear meaning.

Figure 5 shows the magnetization in two representative cases, one for $p=1.068$ (the closest value to $p=1$) and another one for $p=2.007$ (the closest value to $p=2$). Observe that the magnetization in the ferromagnetic slabs has the form a virtual domain wall. The bottom panels show the derivative $\varphi'(z)/q_0$. The discontinuity at $z=100$ is due to the matching condition (31).

B. Thin ferromagnetic slabs

To analyze the case in which the ferromagnetic slabs are very thin slabs we take $q_u(L-L_0)=1$, which means that the thickness of the slabs is equal to the width of a domain wall hosted by a very thick (infinite) magnet. Table II shows that the number of metastable p states is proportional to q_0L_0. The metastable p states are groped into pairs which have very close values of p (see below), and the pairs are homogeneously distributed in the interval $-0.43<p<2.44$. This means that there is a continuum of metastable p states in the limit $q_0L_0\to\infty$. The interval of metastable states is within the limits (41), but does not saturate them. However, these limits are rapidly saturated by increasing the thickness of the slabs, $q_u(L-L_0)$. Indeed, with a thickness equal to twice the domain wall width, $q_u(L-L_0)=2$, the bounds are already saturated.

Figure 6 shows the energy density as a function of p for different values of L_0. For large q_0L_0 the convergence towards the energy density of the magnetic state of the chiral magnet is again observed (see section IV D). It is clearly seen that the metastable p states are grouped into pairs. One of the p states of the pair has lower energy than the infinite chiral magnet limit, while the other has

higher energy. The presence of these metastable higher energy states is due to the thinness of the ferromagnetic slabs. The higher energy states, and thus the pairing, disappear quickly as the thickness of the slabs increases. Indeed it does not appear if $q_u(L - L_0) = 2$.

For illustration, figure 7 shows the magnetization components and the derivative $\varphi'(z)$ for the cases $p = 0.958$ (the closest value to $p = 1$) and $p = 1.997$ (the closest value to $p = 2$), for a chiral magnet of size $q_0 L_0 = 100$. The p state of the left panels is the high energy state of the pair with p closest to 1. We see that the magnetization in the ferromagnetic slab stays very close to the $\hat{y}$ axis, which is perpendicular to the easy axis. This causes the increase of energy density with respect to the infinite chiral magnet case. Since the ferromagnetic slabs are so thin, this increase of energy is not enough to destabilize the state. By contrast, the right panels of figure 7 correspond to the lower energy p state of the pair with p closest to 2. It is seen that, in the ferromagnetic slabs, the magnetization rotates towards the easy axis as we move towards the boundary, and it never crosses the direction perpendicular to the easy axis. The anisotropy energy compensates the ferromagnetic energy due to the rotation and the energy of the composite magnet p state is slightly reduced with respect to the energy of the p state of the infinite chiral magnet.

The bottom panels of figure 7 show the derivative $\varphi'(z)/q_0$. The discontinuity at $z = 100$ is due to the matching condition (31).

VII. CONCLUSIONS

In reference 35 we showed that in an infinite monoaxial chiral magnet there exists a continuum of metastable helical states differing by the helix wave vector, pq_0. It was pointed out that in a real finite magnet only the state with $p = 1$ is compatible with the surface chiral twist induced by the natural boundary conditions [38]. This means that states with $p \neq 1$ are ruled out by the boundary conditions, and, apparently, the results of reference 35 only hold in the non physical cases of an infinite magnet or of a magnet with periodic boundary conditions.

However, the boundary conditions can be taylored by attaching some other magnet to the faces of the monoaxial chiral magnet which are perpendicular to the chiral axis. These magnets may absorb the chiral twist and thus states with different p may satisfy the boundary conditions. We proof in this work that this is indeed the case by considering a composite magnet system formed by a monoaxial chiral magnet attached to two similar slabs of a uniaxial ferromagnet, as in figure 1. We deal only with the case of zero applied field and zero applied current, since this problem can be solved exactly. We show that if the ferromagnets are thick enough (thickness a few tens times larger than the width of their characteristic domain wall) the composite system has metastable magnetic states which are helical within the chiral magnet and look like a virtual domain wall within the ferromagnets (by virtual we mean that the wall center is outside the physical region occupied by the ferromagnetic slab). Those metastable states differ by the wave number of the helix within the chiral magnet and its number increases linearly with size of the chiral magnet, L_0. The results of reference 35 are thus fully recovered in the limit $L_0 \to \infty$.

We also obtain results similar to those of reference 35 (for zero applied field and current) in the limit $L_0 \to \infty$ if the ferromagnetic slabs are thin (thickness approximately equal to the domain wall width). In this case, however, the results are not exactly the same as in 35, since the range of p for which the helical states are metastable is smaller than that predicted in 35.

In reference 35 we pointed out the possibility of using the p states as building blocks for information storing, because there are processes that allow to switch between different p states. In particular, we showed that, in the infinite magnet, the switching between different p states can be performed by applying suitable combinations of external magnetic field and electric current. We expect that some analoguous switching can be also performed in the compositie magnet. In this case, however, the behaviour of the p states under applied field and current has to be studied numerically. Work in this direction is in progress. We expect that the applicacion of an external magnetic field along the chiral axis will deform the p state in the vicinity of the magnet interfaces and will destabilize some of them, gradually, more or less as in the infinite magnet case. Preliminary results confirm this expected behaviour. On the other hand, in the infinite magnet the application of an electric current leads to a rigid steady motion of the p state, and to its destabilization when the current intensity is high enough. In the composite magnet it is difficult to conceive the steady motion state. If the applied current is not too large, we expect a non static, time varying state which retains the helical features of the p state, and an eventual destabilization as the current reaches some critical value, so that, after removing the current, the original p state will be replaced by another one with different p. Then, it seems reasonable to expect that some switching mechanism between p states can be devised for the composite magnet.

Let us stress again a theoretical fact dicussed at the beginning of section V, which may be of interest beyond the physics of chiral magnets. The fact is that, despite appearances, two helical states with very close but different wave numbers are not close in the space of magnetic configurations. In a sense, they are orthogonal, and one cannot be transformed into the other by a small perturbation, no matter how close the wave numbers are [35]. This explains why a helical state cannot reduce its energy by simply changing its wave number: there may be an energy barrier between two helical states even if their wave numbers are arbitrarily close.

At first sight, the existence of so many non degenerate metastable states in chiral magnets is also somehow dis-

concerting, for a different reason: we usually believe that the boundary conditions select one of the many solutions of the differential equations that constrain the state of the system in the static case. In this case, however, if the temperature is low enough and if the energy barriers between the p states are high enough, it is the initial condition what determines the magnetic state in the long term. Actually, this situation resembles the physics of ferromagnets, in which the existence of many metastable states characterized by different spatial distributions of domains is at the origin of hysteresis.

To conclude, let us stress that the possible uses of the p states depend strongly on their life times, which in turn depend on the energy barriers which separate them. If the barriers are high enough, the p states could be experimentally detected at low enough temperature in a composite magnet of the kind studied in this work, for instance with SANS experiments.

ACKNOWLEDGMENTS

We thank M. Garst and J. Masell for pointing out the issues with the boundary conditions and for useful discussions. Grants No. PID2022-138492NB-I00-XM4, funded by MCIN/AEI/10.13039/501100011033, and E11_23R/M4, funded by Diputación General de Aragón, supported this work. This work was also supported by the Grant No. PICT 2017-0906 from the Agencia Nacional de Promoción Científica y Tecnológica, Argentina.

Appendix A: A solution of the double Sine-Gordon equation

The solution of equation (22) which satisfy the conditions (25) can be obtained as follows. Multiplying equation (22) by φ' we get

$$\frac{d}{dz}\left(\varphi'^{\,2} - q_u^2 \sin^2\varphi\right) = 0, \tag{A1}$$

so that the term within brackets has to be a constant. Since we require $\varphi'(L) = 0$ the constant has to be $-q_u^2 \sin^2\varphi_0(L)$ and we obtain

$$\varphi' = q_u \sqrt{\sin^2\varphi - \sin^2\varphi_0(L)}, \tag{A2}$$

since we also require $\varphi' > 0$. Let us call $\eta = \cos\varphi_0(L)$. Notice that $0 < \eta < 1$. Then, solving the above differential equation by separation of variables, we have

$$\int_{-\frac{\pi}{2}}^{\varphi_0} \frac{d\varphi}{\sqrt{\eta^2 - \cos^2\varphi}} = q_u(z - z_0). \tag{A3}$$

With the change of variable $\eta\, t = \cos\varphi$ in the integral, so that $\sin\varphi = -\sqrt{1-\eta^2 t^2}$, we obtain

$$\int_0^{\frac{1}{\eta}\cos\varphi_0} \frac{dt}{\sqrt{(1-t^2)(1-\eta^2 t^2)}} = q_u(z - z_0). \tag{A4}$$

The integral of the left-hand side is

$$\operatorname{arcsn}\big(\cos\varphi_0/\eta, \eta\big), \tag{A5}$$

where $\operatorname{arcsn}(x,\eta)$ is the inverse Jacobi elliptic function [43]. Hence, we get

$$\cos\varphi_0 = \eta\, \operatorname{sn}\big(q_u(z - z_0), \eta\big). \tag{A6}$$

The parameter η is determined by setting $z = L$ in equation (A4), in which case $\cos\varphi_0 = \eta$ and the upper limit of the integral (A4) is one. Thus the integral becomes the complete elliptic integral of the first kind, $K\big(\eta\big)$, so that

$$K\big(\eta\big) = q_u(L - z_0). \tag{A7}$$

The above equation determines uniquely η if L and z_0 are given. Then, since $-\pi < \varphi_0 < 0$, equation (A6) determines completely φ_0, which is given by equation (26). In particular, since $\sin\varphi_0 < 0$, we have

$$\sin\varphi_0 = -\sqrt{1 - \cos^2\varphi_0}. \tag{A8}$$

We also need an explicit form of $\varphi_0'^{\,2}$, which, taking into account (A2) and (A6), has the form

$$\varphi_0'^{\,2}(z) = q_u^2\eta^2\Big(1 - \operatorname{sn}^2\big(q_u(z - z_0), \eta\big)\Big). \tag{A9}$$

Appendix B: Solution of equation (59)

In this appendix we outline a way of solving equation (59) which relies on the Weierstrass elliptic function $\wp$ with fundamental half periods chosen as $\omega_1 = \mathrm{i}\bar{K}$ and $\omega_3 = -K$. We use the notation of reference 47 for the fundamental half periods, and K and $\bar{K}$ are defined in equation (34). This choice of fundamental half periods gives the nome $q = \exp(-\pi K/\bar{K})$, which is convenient if L is large. The related Weierstrass functions ξ and σ and the Jacobi theta functions also appear in the solution. The properties of these functions are thoroughly presented for instance in references 48 or 49, and an exhaustive summary can be found in reference 47. It should be clear that the Weierstrass function ξ of this appendix has nothing to do with the functions ξ_1, ξ_2, and ξ of section V.

Using equation (A2) from appendix A, we see that equation (59) has the form

$$u'' - 2\eta^2 \operatorname{sn}^2(x,\eta) - \big(\beta - 2\eta^2\big)u = 0, \tag{B1}$$

This is one of Lame's equation in Jacobian form [50]. Expressing $\operatorname{sn}(x,\eta)$ in terms of $\wp$, the equation is cast to the form

$$w'' - 2\wp\big(x + \mathrm{i}\bar{K}\big)w - \left(\beta - \frac{2}{3} + \frac{4}{3}(1-\eta^2)\right)w = 0. \tag{B2}$$

For given β, its general solution [50] is a linear combination

$$w(x,\beta) = d_1 w_+(x,\alpha) + d_2 w_-(x,\alpha), \tag{B3}$$

where d_1 and d_2 are arbitrary constants,

$$w_\pm(x,\alpha) = \pm\frac{\sigma(x+\mathrm{i}\bar{K}\pm\alpha)}{\sigma(x+\mathrm{i}\bar{K})\sigma(\alpha)}\,\mathrm{e}^{\pm\xi(\alpha)x}. \tag{B4}$$

and α is the solution of

$$\wp(\alpha) = \beta - \frac{2}{3} + \frac{4}{3}(1-\eta^2), \tag{B5}$$

which, using again the relation between $\mathrm{sn}(x,\eta)$ and $\wp(x)$, leads to equation (69).

If $w'_-(K,\alpha) \neq 0$, the boundary condition $w'(K) = 0$ gives

$$\frac{d_2}{d_1} = -\frac{w'_+(K,\alpha)}{w'_-(K,\alpha)}. \tag{B6}$$

It is convenient to express σ and ξ in terms of theta functions, using equations 23.6.9 and 23.6.13 of reference 47, since these functions have Fourier series rapidly convergent for small q. We get

$$\frac{\sigma(x+\mathrm{i}\bar{K}\pm\alpha)}{\sigma(x+\mathrm{i}\bar{K})\sigma(\alpha)} = \frac{\phi_1'(0,q)\,\phi_1(x+i\bar{K}\pm\alpha,q)}{\phi_1(x+i\bar{K},q)\,\phi_1(\alpha,q)} \times \exp\left(\pm\frac{\xi(\omega_1)}{\omega_1}\alpha(x+\mathrm{i}\bar{K})\right), \tag{B7}$$

$$\xi(\alpha) = \frac{\xi(\omega_1)}{\omega_1}\alpha + \frac{\phi_1'(\alpha,q)}{\phi_1(\alpha,q)}, \tag{B8}$$

where the functions $\phi_i(z,q)$ are related to theta functions by equation (68). We also use the periodicity of the theta functions (formulas 20.2.6 and 20.2.12 of reference 47) to obtain

$$\phi_1\big(z+\mathrm{i}\bar{K}\big) = -\phi_2(z,q). \tag{B9}$$

Inserting equations (B7), (B8) and (B9) into equation (B4), and removing the factor $\exp\big(\mp\xi(\omega_1)\alpha\big)$, which is a pure phase factor of order one as $q\to 0$, what amounts merely to a redefinition of $w_\pm(x,\alpha)$, we obtain equation (67).

The derivatives of $w_\pm(x,\alpha)$ can be readily computed from equation (67), obtaining

$$\frac{w'_\pm(x,\alpha)}{w_\pm(x,\alpha)} = \pm\frac{\phi_2'(x\pm\alpha,q)}{\phi_2(x\pm\alpha,q)} \pm \frac{\phi_2'(x,q)}{\phi_2(x,q)} \mp \frac{\phi_1'(\alpha,q)}{\phi_1(\alpha,q)}. \tag{B10}$$

To compute d_2/d_1, equation (B6), we have to evaluate $w'_\pm\big(K,\alpha\big)$, for which we use the behaviour of theta functions under translation by half periods, given by equation 20.2.13 of reference 47. Taking into account that $\theta_3'(0,q) = 0$ and setting $d_1 = 1$ and $d_2 = d$ we arrive at equation (27).

Appendix C: Expansion in q for large L

1. Case $\beta > 1$

For $q\to 0$ and $\beta > 1 + c$, where $c > 0$ is any fixed number, independent of q, equation (69) can be expanded in powers of q, by introducing the expansion $\alpha = \alpha_0 + \alpha_1 q + \ldots$. Since $\mathrm{sn}(\alpha,\eta) = \tanh(\alpha) + O(q)$, we get for the leading order

$$\alpha_0 = \mathrm{atanh}\left(1/\sqrt{\beta}\right). \tag{C1}$$

It is clear that this expansion is not valid for $\beta\to 1$, since in this limit $\alpha_0\to\infty$.

For $q\to 0$ we have $K = -\log(\sqrt{q}) + O(q\log q)$ and

$$\frac{\pi\alpha}{\bar{K}} = 2\alpha + O(q), \quad \frac{\phi_1'(\alpha,q)}{\phi_1(\alpha,q)} = \sqrt{\beta} + O(q). \tag{C2}$$

Inserting these equations into equation (70) we arrive at equation (72), and we see that d vanishes exponentially as $q_u L\to\infty$. Hence, $w(x,\beta)$ can be approximated by $w_+(x,\alpha)$ in this limit. The expansion of this function in powers of q is obtained from

$$\frac{\phi_1'(0,q)}{\phi_1(\alpha,q)} = 1 + O(q), \quad \frac{\phi_2(x+\alpha,q)}{\phi_2(x,q)} = \sqrt{\beta} - \tanh x + O(q), \tag{C3}$$

and from the second of equations (C2). Inserting these equations into equation (67) for $w_+(x,\alpha)$ we obtain equation (73).

2. Case $\beta = 1$

For $\beta = 1$ the expansion in power of q is different. In this case the right hand side of equation (69) is $1 + O(q)$. Taking into account that $\mathrm{sn}(K,\eta) = 1$, we see that the solution has the form $\alpha = K - \bar{\alpha}$, where $\bar{\alpha}$ is of order one as $q\to 0$. Using the relation $\mathrm{sn}(K-\bar{\alpha},\eta) = \mathrm{cd}(\bar{\alpha},\eta)$, where cd is the ratio of the cn and dn Jacobi elliptic functions, we get the equation for $\bar{\alpha}$,

$$\mathrm{cd}^2(\bar{\alpha},\eta) = 1 - \frac{1-\eta^2}{2-\eta^2}. \tag{C4}$$

Now we can expand this equation in powers of q, inserting the expansion $\bar{\alpha} = \bar{\alpha}_0 + \bar{\alpha}_1 q + \ldots$. Using

$$\mathrm{cd}(\bar{\alpha},q) = 1 - 4\big(\cosh(2\bar{\alpha}) - 1\big)\,q + O(q^2),$$

we obtain $\bar{\alpha}_0 = \mathrm{asinh}\,(\sqrt{2})$.

Then we insert $\alpha = K - \bar{\alpha}$ into the equation for d, (70). We use the properties of theta functions under translations by a half period to obtain

$$\frac{\phi_1'(K-\bar{\alpha})}{\phi_1(K-\bar{\alpha})} = \frac{\pi}{2\bar{K}} - \frac{\phi_4'(\bar{\alpha},q)}{\phi_4(\bar{\alpha},q)}. \tag{C5}$$

Hence, we get

$$d = \exp\left(-\frac{\pi\bar{\alpha}}{\bar{K}} + 2\frac{\phi_4'(\bar{\alpha},q)}{\phi_4(\bar{\alpha},q)}\,K\right). \tag{C6}$$

For $q \to 0$ the term that multiplies K in the exponential is $O(q)$, while K is $O(\log q)$, and therefore d does not vanish as $q \to 0$:

$$d = -\mathrm{e}^{-2\bar{\alpha}_0} + O(q\log q). \tag{C7}$$

For $w_\pm\big(x, K-\bar{\alpha}\big)$ we use the relations

$$\phi_1(K-\bar{\alpha},q) = \mathrm{i}q^{-1/4}\mathrm{e}^{\frac{\pi\bar{\alpha}}{2K}}\phi_4(\bar{\alpha},q), \tag{C8}$$

$$\phi_2(x\pm K\mp\bar{\alpha},q) = q^{-1/4}\mathrm{e}^{\frac{\pi(x\mp\bar{\alpha})}{2K}}\phi_3(x\mp\bar{\alpha},q), \tag{C9}$$

obtained from the behaviour of theta functions under translations of half period. Then we get that, for $\beta = 1$

$$w_\pm\big(x, K-\bar{\alpha}\big) = \pm\frac{\phi_1'(0,q)}{\phi_4(\bar{\alpha},q)}\,\frac{\phi_3(x\pm\bar{\alpha},q)}{\phi_2(x,q)}\times \exp\left(\pm\frac{\phi_4'(\bar{\alpha},q)}{\phi_4(\bar{\alpha},q)}\,x\right). \tag{C10}$$

For $q \to 0$, the above expression gives

$$w_\pm\big(x, K-\bar{\alpha}\big) = (1+\tanh x)\,\mathrm{e}^{-x} + O(q). \tag{C11}$$

Hence, we obtain

$$w(x,\beta=1) = C(1+\tanh x)\,\mathrm{e}^{-x} + O(q\log q), \tag{C12}$$

where $C = 1+\mathrm{e}^{-2\bar{\alpha}_0} = 6-2\sqrt{6} > 0$.

[1] C. Back et al. The 2020 skyrmionics roadmap. *Journal of Physics D: Applied Physics*, 53:363001, 2020.

[2] A. Barman et al. The 2021 Magnonics Roadmap. *J. Phys.: Condens. Matter*, 33:413001, 2021.

[3] M. Mruczkiewicz and P. Gruszecki. The 2021 roadmap for noncollinear magnonics. *Solid State Physics*, 72:1, 2021.

[4] E. Y. Vedmedenko et al. The 2020 magnetism roadmap. *Journal of Physics D: Applied Physics*, 53:453001, 2020.

[5] A. Bogdanov and A. Hubert. The properties of isolated magnetic vortices. *phys. stat. sol. (b)*, 186:527, 1994.

[6] N. Nagaosa and Y. Tokura. Topological properties and dynamics of magnetic skyrmions. *Nat. Nano.*, 8:899, 2013.

[7] I.E. Dzyaloshinskii. Theory of helicoidal structures in antiferromagnets. I. Nonmetals. *Sov. Phys. JETP*, 19:960, 1964.

[8] J. Kishine and A.S. Ovchinnikov. Theory of monoaxial chiral helimagnet. *Solid State Physics*, 66:1–130, 2015.

[9] P. Bak and M.H. Jensen. Theory of helical magnetic structures and phase transitions in mnsi and fege. *Journal of Physics C: Solid State Physics*, 13(31):L881–L885, 1980.

[10] T. Miyadai, K. Kikuchi, H. Kondo, S. Sakka, M. Arai, and Y. Ishikawa. Magnetic properties of $Cr_{1/3}NbS_2$. *J. Phys. Soc. Jpn.*, 52:1394, 1983.

[11] Y. Togawa, T. Koyama, T. Takayanagi, S. Mori, Y. Kousaka, J. Akimitsu, S. Nishihara, K. Inoue, A.S. Ovchinnikov, and J. Kishine. Chiral magnetic soliton lattice on a chiral helimagnet. *Phys. Rev. Lett.*, 108:107202, 2012.

[12] V. Laliena, J. Campo, J. Kishine, A.S. Ovchinnikov, Y. Togawa, Y. Kousaka, and K. Inoue. Incommensurate-commensurate transitions in the mono-axial chiral helimagnet driven by the magnetic field. *Phys. Rev. B*, 93:134424, 2016.

[13] V. Laliena, J. Campo, and Y. Kousaka. Understanding the H-T phase diagram of the monoaxial helimagnet. *Phys. Rev. B*, 94:094439, 2016.

[14] V. Laliena, J. Campo, and Y. Kousaka. Nucleation, instability, and discontinuous phase transitions in the phase diagram of the monoaxial helimagnet with oblique fields. *Phys. Rev. B*, 95:224410, 2017.

[15] N.J. Ghimire, M.A. McGuire, D.S. Parker, B. Sipos, S. Tang, J.-Q. Yan, B.C. Sales, and D. Mandrus. Magnetic phase transition in single crystals of the chiral helimagnet $Cr_{1/3}NbS_2$. *Phys. Rev. B*, 87:104403, 2013.

[16] B.J. Chapman, A.C. Bornstein, N.J. Ghimire, D.G. Mandrus, and M. Lee. Spin structure of the anisotropic helimagnet $Cr_{1/3}NbS_2$ in a magnetic field. *Appl. Phys. Lett.*, 105:072405, 2014.

[17] K. Tsuruta, M. Mito, H. Deguchi, J. Kishine, Y. Kousaka, J. Akimitsu, and K. Inoue. Phase diagram of the chiral magnet $Cr_{1/3}NbS_2$ in a magnetic field. *Phys. Rev. B*, 93:104402, 2016.

[18] Jun-ichiro Yonemura, Yusuke Shimamoto, Takanori Kida, Daichi Yoshizawa, Yusuke Kousaka, Sadafumi Nishihara, Francisco Jose Trindade Goncalves, Jun Akimitsu, Katsuya Inoue, Masayuki Hagiwara, and Yoshihiko Togawa. Magnetic solitons and magnetic phase diagram of the hexagonal chiral crystal $CrNb_3S_6$ in oblique magnetic fields. *Phys. Rev. B*, 96:184423, 2017.

[19] Eleanor M. Clements, Raja Das, Ling Li, Paula J. Lampen-Kelley, Manh-Huong Phan, Veerle Keppens, David Mandrus, and Hariharan Srikanth. Critical behavior and macroscopic phase diagram of the monoaxial chiral helimagnet $Cr_{1/3}NbS_2$. *Sci. Rep.*, 7:6545, 2017.

[20] E.M. Clements, R. Das, M.-H. Phan, L. Li, V. Keppens, D. Mandrus, M. Osofsky, and H. Srikanth. Magnetic field dependence of nonlinear magnetic response and tricritical point in the monoaxial chiral helimagnet $Cr_{1/3}NbS_2$. *Phys. Rev. B*, 97:214438, 2018.

[21] S. A. Osorio, V. Laliena, J. Campo, and S. Bustingorry. Chiral helimagnetism and stability of magnetic textures in $MnNb_3S_6$. *Phys. Rev. B*, 108:054414, 2023.

[22] V. Laliena, S. Bustingorry, and J. Campo. Dynamics of chiral solitons driven by polarized currents in monoaxial helimagnets. *Sci. Rep.*, 10:20430, 2020.

[23] T. Moriya and T. Miyadai. Evidence for the helical spin structure due to antisymmetric exchange interaction in $Cr_{1/3}NbS_2$. *Solid State Commun.*, 42:209, 1982.

[24] J. Kishine, K. Inoue, and Y. Yoshida. Synthesis, struc-

ture and magnetic properties of chiral molecule-based magnets. *Prog. Theor. Phys.*, 159:82, 2005.

[25] Y. Kousaka, T. Ogura, J. Zhang, P. Miao, S. Lee, S. Torii, T. Kamiyama, J. Campo, K. Inoue, and J. Akimitsu. Long periodic helimagnetic ordering in CrM_3S_6 (M = Nb and Ta). *J. of Phys.: Conf. Series*, 746:012061, 2016.

[26] Sunil K. Karna, F. N. Womack, R. Chapai, D. P. Young, M. Marshall, Weiwei Xie, D. Graf, Yan Wu, Huibo Cao, L. DeBeer-Schmitt, P. W. Adams, R. Jin, and J. F. DiTusa. Consequences of magnetic ordering in chiral $Mn_{1/3}Nbs_2$. *Phys. Rev. B*, 100:184413, 2019.

[27] B. Roessli, J. Schäfer, G. A. Petrakovskii, B. Ouladdiaf, M. Boehm, U. Staub, A. Vorotinov, and L. Bezmaternikh. Formation of a magnetic soliton lattice in copper metaborate. *Phys. Rev. Lett.*, 86:1885–1888, 2001.

[28] Kimio Adachi, Norio Achiwa, and Mamoru Mekata. Helical magnetic structure in $CsCuCl_3$. *J. Phys. Soc. Jpn.*, 49:545–553, 1980.

[29] S. Ohara, S. Fukuta, K. Ohta, H. Kono, T. Yamashita, Y. Matsumoto, and J. Yamaura. Study of chiral structure and magnetism in heavy-fermion $Yb(Ni_{1-x}Cu_x)_3Al_9$. *JPS Conf. Proc.*, 3:017016, 2014.

[30] T. Matsumura, Y. Kita, K. Kubo, Y. Yoshikawa, S. Michimura, T. Inami, Y. Kousaka, K. Inoue, and S. Ohara. Chiral soliton lattice formation in monoaxial helimagnet $Yb(Ni_{1-x}Cu_x)_3Al_9$. *J. Phys. Soc. Jpn.*, 86:124702, 2017.

[31] A. Zheludev, S. Maslov, G. Shirane, Y. Sasago, N. Koide, and K. Uchinokura. Field-induced commensurate-incommensurate phase transition in a Dzyaloshinskii-Moriya spiral antiferromagnet. *Phys. Rev. Lett.*, 78:4857–4860, 1997.

[32] Jan Masell, Xiuzhen Yu, Naoya Kanazawa, Yoshinori Tokura, and Naoto Nagaosa. Combing the helical phase of chiral magnets with electric currents. *Phys. Rev. B*, 102(18):180402, 2020.

[33] Fehmi Sami Yasin, Jan Masell, Kosuke Karube, Daisuke Shindo, Yasujiro Taguchi, Yoshinori Tokura, and Xiuzhen Yu. Heat current-driven topological spin texture transformations and helical q-vector switching. *Nature Communications*, 14(1), 2023.

[34] N.T. Bechler and J. Masell. Helitronics as a potential building block for classical and unconventional computing. *Neuromorphic Computing and Engineering*, 3(3), 2023.

[35] V. Laliena, S. A. Osorio, D. Bazo, S. Bustingorry, and J. Campo. Continuum of metastable conical states in monoaxial helimagnets. *Phys. Rev. B*, 108:024425, 2023.

[36] V. Laliena, Y. Kato, G. Albalate, and J. Campo. Thermal fluctuations in the conical state of monoaxial helimagnets. *Phys. Rev. B*, 98:144445, 2018.

[37] V. Laliena and J. Campo. Stability of skyrmion textures and the role of thermal fluctuations in cubic helimagnets: a new intermediate phase at low temperature. *Phys. Rev. B*, 96:134420, 2017.

[38] Markus Garst. Private communication.

[39] C. Abert. Micromagnetics and spintronics: models and numerical methods. *Eur. Phys. J. B*, 92:120, 2019.

[40] Paul Heistracher, Claas Abert, Florian Bruckner, Thomas Schrefl, and Dieter Suess. Proposal for a micromagnetic standard problem: Domain wall pinning at phase boundaries. *J. Mag. Mag. Mat.*, 548:168875, 2022.

[41] A. Hubert and R. Schäfer. *Magnetic Domains*. Springer-Verlag, Berlin Heidelberg New York, 2008.

[42] Notice that, in the realm of elliptic functions, the conventional notation for what we call $\bar{K}$ is K'. We depart from the conventional notation to avoid confusion, since we use the prime for derivatives.

[43] I. S. Gradshteyn and I. M. Ryzhik. *Tables of Integrals, Series, and Products*. Academic Press, 2007.

[44] C. Kittel. Physical theory of ferromagnetic domains. *Rev. Md. Phys.*, 21:541, 1949.

[45] J. Weidmann. *Spectral Theory of Ordinary Differential Operators*. Springer-Verlag, Berlin Heidelberg New York, 1987.

[46] The maximal domain of these operators, where they are selfadjoint, is the set of absolutely continuous functions u such that au' is also absolutely continuous [45].

[47] F. W. J. Olver, A. B. Olde Daalhuis, D. W. Lozier, B. I. Schneider, R. F. Boisvert, C. W. Clark, B. R. Miller, B. V. Saunders, H. S. Cohl, and M. A. McClain. NIST Digital Library of Mathematical Functions. `https://dlmf.nist.gov/`. Release 1.1.10 of 2023-06-15.

[48] E.T. Whittaker and G.N. Watson. *A Course of Modern Analysis*. Cambridge University Press, New York, 1927.

[49] N. I. Akhiezer. *Elements of the Theory of Elliptic Functions*. American Mathematical Society, Providence, 1990.

[50] F. M. Arscott. *Periodic diifferential equations. An introduction to Mathieu, Lamé, and allied functions*, volume 66 of *International Series of Monographs in Pure and Applied Mathematics*. Pergamon Press, New York, 1964.